# Multiscale modeling of oxygen diffusion through the oxide during silicon oxidation

Angelo Bongiorno* and Alfredo Pasquarello

*Institut de Théorie des Phénomènes Physiques (ITP), Ecole Polytechnique Fédérale de Lausanne (EPFL),*
*CH-1015 Lausanne, Switzerland*
*and Institut Romand de Recherche Numérique en Physique des Matériaux (IRRMA), CH-1015 Lausanne, Switzerland*

We investigate at the atomic scale the oxygen diffusion process occurring during silicon oxidation. First, we address the energetics of several oxygen species in the oxide using density-functional calculations. Our results support the interstitial $O_2$ molecule as the most stable oxygen species. We then adopt a classical scheme for describing the energetical and topological properties of the percolative diffusion of the $O_2$ molecule through the interstitial network of the oxide. By studying a large set of disordered oxide structures, we derive distributions of energy minima, transition barriers, and the number of connections between nearest-neighbor minima. These distributions are then mapped onto a lattice model to study the long-range $O_2$ diffusion process by Monte-Carlo simulations. The resulting activation energy for diffusion is found to be in agreement with experimental values. We also extend our atomic-scale approach to an oxide of higher density, finding a significant decrease of the diffusivity. To address the $O_2$ diffusion directly at the $Si$-$SiO_2$ interface, we construct a lattice model of the interface which incorporates the appropriate energetic and connectivity properties in a statistical way. In particular, this lattice model shows a thin oxide layer of higher density at the interface, in accord with x-ray reflectivity data. We carry out Monte-Carlo simulations of the $O_2$ diffusion for this model and obtain the dependence of the diffusion rate on oxide thickness. For oxide thicknesses down to about 2 nm, we find that the presence of an oxide layer of higher density at the $Si$-$SiO_2$ interface causes a drop of the $O_2$ diffusion rate with respect to its value in bulk $SiO_2$, in qualitative agreement with the observed oxidation kinetics.

## I. INTRODUCTION

Silicon dioxide ($SiO_2$) films thermally grown on crystalline silicon (Si) substrates constitute the principal gate dielectrics in metal-oxide-semiconductor devices.[1] Nowadays, gate dielectrics implemented in very-large scale integration manufacturing are between 2 and 9 nm thick.[2–4] Designing modern processing routes for the formation of thin dielectric layers requires not only a very precise knowledge of the growth kinetics but also an atomic-scale understanding of the microscopic processes which lead to the formation of the $Si$-$SiO_2$ interface.

According to the model introduced by Deal and Grove,[5] the formation of a thermal oxide film on silicon is supposed to proceed through three sequential steps: (i) the insertion of an oxygen species from the vacuum into a preexisting oxide layer; (ii) the diffusion of the oxidant species through the disordered oxide network toward the Si substrate, and finally (iii) the oxidizing reaction at the interface, where the new oxide is formed.[5] The Deal-Grove model has proved to be extremely successful in reproducing a large variety of experimental data on the kinetics of the silicon oxidation process.[5–8] In particular, the Deal-Grove model describes accurately the growth kinetics of thick oxide films.[5–8] In this regime, the oxidation kinetics is governed by the oxygen diffusion process. Kinetics data show that the oxygen solubility depends linearly on pressure and that the activation energy for oxygen diffusion is around 1.2 eV.[5–8] These observations are in agreement with early oxygen permeation experiments on silica membranes.[9]

Assuming a first-order reaction between external gaseous $O_2$ and the dissolved oxygen species in $SiO_2$, Deal and Grove naturally identified the undissociated oxygen molecule as the diffusing species during silicon oxidation.[5] Furthermore, by similarity with argon, an atom of approximately the same size and activation energy for diffusion in silica,[10] the $O_2$ molecule was supposed to migrate through the interstices of the oxide network.[5]

Direct experimental observations generally support the Deal-Grove description of the oxygen diffusion process. Indeed, nuclear reaction resonance,[11–14] secondary ion mass spectrometry,[15] and medium energy ion scattering experiments[16] based on $^{16}O$-$^{18}O$ sequential oxidation all confirm that the bulk of the oxide does not incorporate oxygen during oxidation and that the new oxide essentially grows at the $Si$-$SiO_2$ interface. However, these experiments also revealed the occurrence of oxygen exchange processes at the external $SiO_2$ surface. More recently, oxygen exchange processes were also found to occur at the $Si$-$SiO_2$ interface,[17,18] providing support to an interpretation of the oxidation process which favors atomic oxygen as the transported species through the oxide.[19]

Different atomic-scale mechanisms have so far been proposed for the diffusion of the $O_2$ molecule in amorphous $SiO_2$ ($a$-$SiO_2$).[20–22] Mott invoked a mechanism based on the availability of two kinds of local minima,[20,21] while Revesz and Schaeffer assumed the existence of special diffusive channels through the oxide.[22] However, such mechanisms appear unsatisfactory, since they both contrast with the homogeneous nature of a continuous random network, generally assumed as structural model of $a$-$SiO_2$.

Theoretical investigations based on density functional theory appear particularly suitable for providing insight in atomic processes involving oxygen species in $SiO_2$.[23–32] So far, many studies have been devoted to investigating the relative energetics of both neutral and charged oxygen species in $\alpha$-quartz.[23–27,30,32] This crystalline model has also been adopted to study the diffusion properties of the peroxyl linkage,[23,26] an oxygen atom incorporated in a Si-O-Si unit. More recently, the effect of the disordered nature of the oxide on the energetics of the several oxygen species has been addressed.[28,29] However, attempts at understanding the oxygen migration reduce to the calculation of transition barriers for the diffusion of the interstitial $O_2$ molecule along a limited amount of pathways.[29,32]

We recently reported in a concise form on an atomic-scale investigation of the oxygen diffusion process through the oxide layer during silicon oxidation.[33] We elucidated the nature of the diffusing oxygen species in $a$-$SiO_2$ and the physical mechanism underlying this process. We adopted in sequence first-principles calculations, classical molecular dynamics, and Monte-Carlo simulations to span the relevant length and time scales for an appropriate description of the long-range diffusion process in a disordered network. The present paper complements our previous work in two ways. First, we now provide a more detailed description of the adopted methodologies and of the obtained results. Second, we extend our work to the $O_2$ diffusion across an oxide layer at the Si-$SiO_2$ interface accounting for the effect of an interfacial layer of higher density.[34,35]

The paper is organized as follows. In Sec. II, we study the energetics of several oxygen species in the oxide. In Sec. III, we derive a classical scheme for the energetics of the interstitial $O_2$ molecule in $a$-$SiO_2$. This scheme then allows us to provide a statistical description of the energetical and topological properties of the potential energy landscape for $O_2$ diffusion in $a$-$SiO_2$. In Sec. IV, we describe our Monte-Carlo simulations on lattice models for investigating the long-range diffusion process. In Sec. V, we first extend our approach for studying the oxygen diffusion to a bulk oxide of higher density. Then, we obtain the oxygen diffusion rate as a function of oxide thickness at the Si-$SiO_2$ interface, accounting for the effect of an interfacial oxide layer of higher density. Conclusions are drawn in Sec. VI.

## II. ENERGETICS OF OXYGEN SPECIES IN SILICON DIOXIDE

Thick oxide films ($>20$ nm) are opaque to electrons. Electrons or holes might be introduced in the oxide from the conduction or the valence band of the silicon substrate. However, both the conduction-band and the valence-band offsets ($\sim 3$ and $\sim 4.5$ eV,[36] respectively) correspond to high energy barriers which prevent charge carriers to flow through the oxide layer, even at the relatively high temperatures of the oxidation process. In addition, experimental studies on thick films have shown that growth rates are independent of electric fields, thereby ruling out charged oxygen species as oxidizing agents during silicon oxidation.[37–41] For these reasons, we focus in the present investigation only on neutral oxygen species.
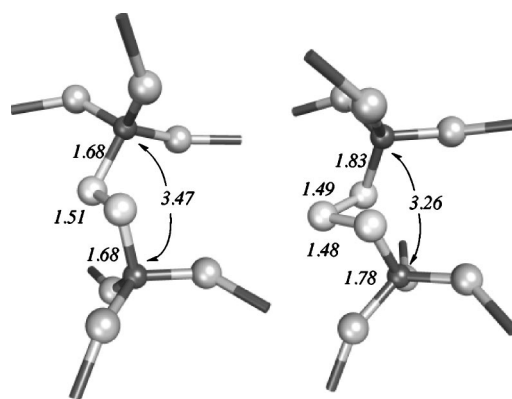


FIG. 1. Peroxyl (left) and ozonyl (right) linkages in $\alpha$-quartz. Some bond distances are indicated. Dark and light balls represent Si and O atoms, respectively.

The incorporation of oxygen from the gas phase in the oxide layer can lead to the formation of either molecular or, upon dissociation, atomic oxygen species. In particular, an additional O atom or $O_2$ molecule could incorporate in a Si-O-Si unit of the $SiO_2$ network forming a peroxyl or an ozonyl linkage, respectively (Fig. 1).[23,25] Alternatively, these atomic and molecular oxygen species could find equilibrium positions in the interstices of the $SiO_2$ network (Fig. 2). All these oxygen species have been suggested to play an important role during silicon oxidation.[5,14,19,23,25] In the following, we will focus on their energetics in $SiO_2$. The formation energy of an oxygen species within the oxide will be referred to the isolated $O_2$ molecule and the unperturbed oxide.

### A. First-principles scheme

To accurately describe the energetics of oxygen species in $SiO_2$, we adopt a first-principles scheme based on density-functional theory.[42,43] The exchange and correlation energy is accounted for within a generalized gradient approximation.[44,45] Only valence wave functions are described explicitly while pseudopotentials are used to account for core-valence interactions. We use a norm-conserving pseudopotential for Si, derived as in Ref. 46, and an ultrasoft pseudopotential for O.[47] Plane-wave energy cutoffs of 24 and 150 Ry are used for the wave functions and the augmented
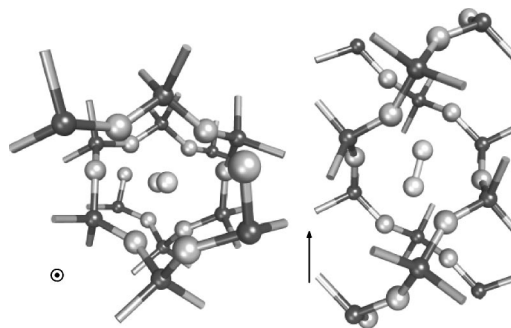


FIG. 2. Interstitial molecular oxygen in $\alpha$-quartz. The left (right) panel gives a view along a direction parallel (orthogonal) to the $c$ axis. Dark and light balls represent Si and O atoms, respectively.

electron density, respectively.[48,49] Only the $\Gamma$-point is used to sample the Brillouin zone. Full structural relaxations are carried out using a damped molecular dynamics scheme.[50] We use a spin-polarized functional to accurately describe the electronic ground state of the oxygen molecule, either in vacuum (its ground state is $^3\Sigma_g$) or in $SiO_2$.[27,51] For the isolated $O_2$ dimer we find a bond length of 1.26 Å, a dissociation energy of 5.68 eV (the zero-point vibrational energy correction being included), and a vibrational frequency of 1541 cm$^{-1}$, to be compared with the respective experimental values of 1.22 Å, 5.1 eV and 1578 cm$^{-1}$.[52]

### B. Oxygen species in $\alpha$-quartz

Most theoretical studies usually adopt $\alpha$-quartz, the most stable crystalline phase of $SiO_2$ at standard ambient conditions, as a model for $a$-$SiO_2$.[23–27,31] To allow a comparison with previous theoretical studies, we first investigate the relative energetics of oxygen species in this crystalline material. To model $\alpha$-quartz, we use a periodic orthorhombic cell containing 72 atoms with fixed cell parameters of 9.94 Å $\times 8.61$ Å $\times 10.91$ Å, corresponding to the theoretical lattice constants.[53]

We find that the interstitial $O_2$ molecule with spin $S=1$ is the most stable oxygen species in $\alpha$-quartz. The $O_2$ molecule is found to be approximately oriented along the $c$ axis, showing a small tilt of 14° (Fig. 2). Upon relaxation, the nearby Si and O atoms of the $\alpha$-quartz network move away from the $O_2$ molecule by 0.1–0.2 Å and 0.2–0.5 Å, respectively. The energy of the interstitial $O_2$ is found to be higher than that of the free molecule by 3.4 eV. The spin state $S=0$ is found to be higher than the $S=1$ state by 0.3 eV. The interstitial molecular species with $S=1$ is found to be considerably more stable than two separated interstitial O atoms in $\alpha$-quartz. In particular, we find energy differences of 3.2 eV and 3.4 eV for the interstitial O atoms in the singlet and triplet spin state, respectively.

The network oxygen species are found at higher energies with respect to the interstitial $O_2$ molecule. We find an increase of 1.0 and 1.6 eV per pair of O atoms for the ozonyl and the peroxyl linkages, respectively. The relaxed atomic structures of these configurations are illustrated in Fig. 1. The lower energy of the ozonyl linkage with respect to the peroxyl bridge is consistent with the distance between the Si atoms which accommodate these oxygen species. For the peroxyl bridge this distance is found to be 3.47 Å, significantly longer than in the nondefected $\alpha$-quartz model (3.09 Å). The ozonyl linkage gives rise to a Si-Si distance of 3.26 Å, indicating that this species can be more easily accommodated in the $\alpha$-quartz network.

Our results show very good agreement with recent first-principles calculations.[24,26,27,31] However, the comparison with two early first-principles investigations reveals differences which cannot simply be attributed to technicalities.[23,25] In fact, these early studies neglected spin polarization effects,[23,25] which were later found to be important for accurately accounting for the energy of the interstitial $O_2$ molecule in $SiO_2$.[27] In addition, in Ref. 23, the calculated energy levels for oxygen in $\alpha$-quartz were also affected by the use of

TABLE I. A comparison between average structural parameters of amorphous $SiO_2$ at regular density ($a$-$SiO_2$) and of amorphous $SiO_2$ at higher density ($d$-$SiO_2$), as obtained by classical molecular dynamics. The standard deviations are given after the $\pm$ sign.

| | $a$-$SiO_2$ | $d$-$SiO_2$ |
|---|---|---|
| $\rho$ (g/cm$^3$) | 2.2 | 2.4 |
| Si–Si (Å) | $3.12\pm0.08$ | $3.08\pm0.12$ |
| Si–O (Å) | $1.61\pm0.02$ | $1.61\pm0.02$ |
| O–O (Å) | $2.63\pm0.09$ | $2.63\pm0.09$ |
| $\angle$Si-O-Si | $152°\pm12°$ | $149°\pm13°$ |
| $\angle$O-Si-O | $109.4°\pm5.8°$ | $109.4°\pm5.8°$ |

a small simulation cell. These aspects have been critically addressed in Ref. 30.

### C. Model structures of $a$-$SiO_2$

We adopt a classical molecular dynamics scheme to generate a set of independent model structures representing the oxide. In this scheme, the interactions between Si and O atoms are described by the interatomic potentials given in Ref. 54. We use periodically repeated cubic cells of fixed volume, corresponding to the experimental density of silica (2.2 g/cm$^3$). Starting from random atomic positions, models of liquid $SiO_2$ are equilibrated at 3500 K for more than 300 ps. Amorphous structures are then obtained by quenching from the melt with a cooling rate of approximately 7 K/ps.[55] Full simulations last from 500 ps to 1 ns, depending on the size of the model structure. We construct a large set of model structures containing between 72 and 144 atoms in the periodic cell. The full set of models spans an equivalent bulk volume of 574 $SiO_2$ units.

All the model structures of the oxide consist of a random network of corner-sharing tetrahedral $SiO_4$ units without coordination defects. The structural parameters reported in Table I confirm that the model structures reproduce the typical short-range order of $a$-$SiO_2$. Indeed, the mean value of 152° for the Si-O-Si bond angle distribution and the relative standard deviation of 12° compare well with the corresponding values extracted from x-ray diffraction (148° and 13°) or NMR data (151° and 11°).[56,57] In addition, the calculated structure factor compares well with neutron diffraction data and shows the characteristic first sharp diffraction peak at about 1.5 Å$^{-1}$.[58] The agreement stems from a proper description of the intermediate range order of $a$-$SiO_2$, even in our smallest model structures (Fig. 3).

The ring statistics averaged over the full set of model structures is extracted according to the shortest path analysis,[59] and is reported in Fig. 4. Our results compare well with distributions obtained for larger model structures of $a$-$SiO_2$, generated by similar approaches.[55,60] In addition, the concentrations of oxygen atoms in three- and fourfold rings, 1.2% and 5.3%, respectively, are in fair agreement with recent theoretical estimates derived from Raman spectra of vitreous silica (0.26% and 1.0%).[61]

### D. Oxygen species in $a$-$SiO_2$

We choose two specific 72-atom model structures of $a$-$SiO_2$ for evaluating the energetics of various oxygen species
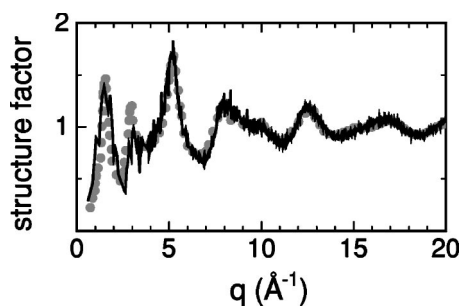
FIG. 3. Calculated structure factor (solid) for model structures of amorphous $SiO_2$ at regular density containing 72 atoms, compared to experimental data from Ref. 58. Larger models show a similar level of agreement.

within our density functional scheme. One of these model structures was taken from the large set generated in Sec. II C. The other one had been generated previously by first-principles molecular dynamics.[62,63] Structural differences between the two models are essentially limited to the ring statistics and to the distribution of interstitial volumes.

Our study encompasses the interstitial $O_2$ molecule and the two network species, the peroxyl and ozonyl linkages. We disregard the interstitial atomic species on the basis of its high formation energy in $\alpha$-quartz. To account for the statistical variety of sites, we introduce the oxygen molecule within the available interstitial cages offered by the network, while, for the peroxyl and ozonyl linkage, we select a set of Si-O-Si units showing different bond angles for constructing their initial configuration. The defected structures are then relaxed within the first-principles scheme.

We find energies for the network species, the peroxyl and ozonyl linkages, spread around the values calculated for $\alpha$-quartz. We find energies ranging between 3.4 eV and 5.5 eV for the peroxyl linkage, and between 2.4 eV and 4.7 eV for the ozonyl linkage. For both network species, energies do not show any apparent correlation with the Si-O-Si bond angle of the undefected $SiO_2$ structure.[28] At variance, the energy of the interstitial $O_2$ molecule shows a strong correlation with the size of the interstitial void, strongly decreasing for increasing cage sizes (Fig. 5).

For selected configurations involving the interstitial $O_2$ molecule, we also evaluate the energy difference between the triplet and the singlet spin states. In the set of considered configurations, we include both typical equilibrium states
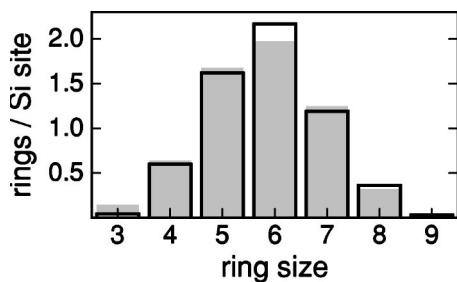


FIG. 4. Average ring statistics in model structures of amorphous $SiO_2$ at regular density (shaded histogram) and of amorphous $SiO_2$ at a density of 2.4 g/cm³ (thick solid line).
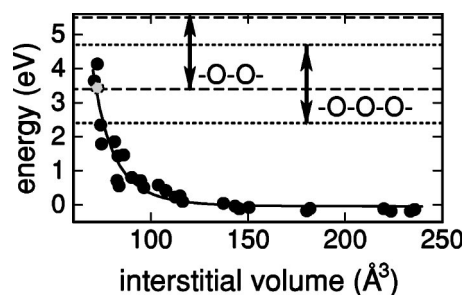


FIG. 5. Energies of the interstitial $O_2$ molecule, and of the peroxyl (-O-O-) and ozonyl (-O-O-O-) linkages in $a$-$SiO_2$, as obtained within a density-functional approach. The energy of the interstitial $O_2$ molecule (disks) is reported vs the volume of the largest ellipsoidal void centered on the molecule. The solid line is a guide to the eye. For comparison, the energy of the interstitial $O_2$ molecule in $\alpha$-quartz is also reported (gray disk). The range of energies corresponding to peroxyl (O-O) and ozonyl (O-O-O) linkages are indicated.

and typical transition states for $O_2$ migration (cf. Sec. III B). We always find that the singlet state is at higher energies than its corresponding triplet state, by approximately the same amount ($\sim$0.3 eV) as in $\alpha$-quartz. This result is in qualitative agreement with a recent study on the way the spin affects the $O_2$ diffusion in $\alpha$-quartz.[27]

### E. Distribution of voids in $a$-$SiO_2$

In the previous section, we have seen that the energy of the interstitial $O_2$ molecule depends on the size of the available interstitial voids (Fig. 5). It is therefore important to characterize the interstitial void distribution in $a$-$SiO_2$. Several purposes motivate this characterization: (i) to determine the relative stability of the interstitial $O_2$ molecule with respect to other oxygen species, (ii) to estimate the concentration of equilibrium sites for $O_2$, and (iii) to examine whether a diffusion mechanism based on the hopping of an $O_2$ molecule between such sites is possible.

In this section, we address these issues carrying out an analysis relying solely on geometric criteria. Further on, we will support the main conclusions of this analysis by energetic considerations. We use the extended set of continuous random network models of $a$-$SiO_2$ generated in Sec. II C and derive the interstitial void distribution on the basis of a geometric Voronoi analysis (see Refs. 64,65, and references therein).

The Voronoi analysis of a disordered network consists of partitioning the space in polyhedra, each containing the volume nearest a given atom. The vertices of these polyhedra have the property of being equidistant to at least four atoms of the $SiO_2$ network. Thus, the Voronoi analysis of a disordered distribution of atoms directly leads to the definition of spheres characterizing the distribution of interstitial voids. Recently, this definition of interstitial voids has also been used to investigate the origin of the first sharp diffraction peak appearing in the structure factor of disordered network-forming materials.[65,66]

We applied the Voronoi analysis on both $\alpha$-quartz and on our set of model structures of $a$-$SiO_2$ [Fig. 6(a)]. Interstitial
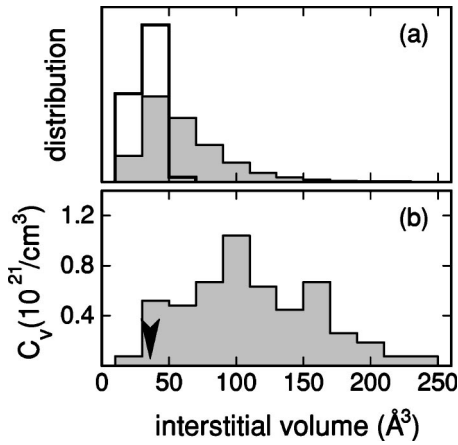
FIG. 6. (a) Distribution of interstitial volumes in $\alpha$-quartz (thick-solid line, open histogram) and in the model structures of $a$-SiO$_2$ generated in this work (filled histogram). The interstitial voids are defined using a Voronoi analysis. (b) Concentration of interstitial voids, extracted by the Voronoi analysis, whose center is not included in a void of larger radius. The arrow gives the result for $\alpha$-quartz.

voids in $\alpha$-quartz show volumes closely distributed around 33 Å$^3$. In $a$-SiO$_2$, the distribution of volumes is shifted toward higher values (an average volume of 58 Å$^3$), and is remarkably broader. However, it appears unreasonable to associate, on a one to one basis, interstitial voids defined in this way to equilibrium sites for the O$_2$ molecule. In fact, careful inspection of the set of such interstitial voids shows that the centers of a large number of voids are located within voids of a larger radius. Since such smaller voids are presumably all associated to the same equilibrium site for the interstitial O$_2$ molecule, it is physically more reasonable to omit these voids from the considered set.

The retained interstitial voids give the distribution of volumes shown in Fig. 6(b). In $\alpha$-quartz, this procedure gives a single volume (33 Å$^3$). In the amorphous models, most of the interstitial voids now have volumes larger than in $\alpha$-quartz, showing an average volume of about 110 Å$^3$, corresponding to interstitials where, in view of the results in Fig. 5, the O$_2$ molecule has energies less than 1 eV. This suggests that these voids are good candidates for equilibrium sites of the interstitial O$_2$ molecule. Moreover, we note that only in a small fraction of interstitial voids the O$_2$ molecule has energies comparable to those of the network species. This occurs for interstitial volumes close to those in $\alpha$-quartz [Fig. 5 and Fig. 6(b)]. The fact that most of the interstitials in $a$-SiO$_2$ are significantly larger than in $\alpha$-quartz suggests that O$_2$ is the most stable neutral oxygen species in $a$-SiO$_2$.

From the void distribution reported in Fig. 6(b), we derive the value of $5.1 \times 10^{21}$ cm$^{-3}$ for the concentration of equilibrium sites of O$_2$ in $a$-SiO$_2$. By considering voids with overlapping spheres as nearest neighbors, we find an average distance between nearest neighbor equilibrium sites of 4.7 Å. The size of this distance is consistent with a diffusion mechanism based on hopping events of the O$_2$ molecule between equilibrium sites. This consideration is solely based on the distribution of equilibrium sites. A conclusive assessment requires the study of the potential energy landscape connecting these sites.

TABLE II. Parameters of the Lennard-Jones-like interatomic potentials describing the interaction between the interstitial O$_2$ molecule and the SiO$_2$ network.

| $x$ | $\epsilon$ (eV) | $\sigma$ (Å) | $n$ | $\gamma$ (eV) | $\rho$ (Å) |
|-----|-----------------|--------------|-----|---------------|------------|
| O  | 2.46 | 1.99 | 7 | 1.07 | 2.11 |
| Si | 1.44 | 1.99 | 9 | 0.39 | 0.37 |

## III. POTENTIAL ENERGY LANDSCAPE FOR O$_2$ DIFFUSION IN SILICA

Amorphous SiO$_2$ offers a variety of interstitials as equilibrium sites for O$_2$. The transition energies required for going from a local minimum to neighboring ones depend on the local environment. Such equilibrium sites are not expected to be equivalent, showing different local energies and transition barriers. Furthermore, the number of viable connections to reach a given equilibrium site is also expected to show statistical variation. Hence, to address the O$_2$ diffusion process in $a$-SiO$_2$, we need to explore both the energetical and topological properties of the interstitial network available for O$_2$ diffusion. Treating the statistical diversity within a first-principles approach constitutes at present a prohibitive computational effort. Therefore, it is necessary to resort to a simpler and computationally more advantageous scheme.

### A. Classical scheme

To extensively sample the properties of the disordered interstitial network for the diffusion of the O$_2$ molecule in $a$-SiO$_2$, we construct a simplified energy scheme based on classical interatomic potentials. For the Si and O atoms of the SiO$_2$ network, we adopt the same interatomic potentials as used for generating the model structures of $a$-SiO$_2$ (Sec. II C), while we derive a new set of potentials to account for the interaction between the O$_2$ molecule and the oxide network. In particular, the interaction between the O atoms within the molecule is described by a Morse potential whose parameters are directly obtained from the bond length, the dissociation energy, and the harmonic force-constant calculated from first-principles (Sec. II A).

For the O$_2$-SiO$_2$ interaction, we adopt Lennard-Jones-like potentials. More precisely, for each oxygen atom $i$ ($i = 1, 2$) of the O$_2$ molecule, the potential,

$$V_x^i = \epsilon_x \left( \frac{\sigma_x}{r_{ix}} \right)^{n_x} - \gamma_x \left( \frac{\rho_x}{r_{ix}} \right)^6, \tag{1}$$

describes the interaction with a network atom of species $x$, where $x =$ Si or O. $n_x$ is taken to be 7 and 9 for $x =$ O and Si, respectively. We fix the other parameters by fitting the energies obtained within our first principles scheme for the O$_2$ molecule at equilibrium sites in $a$-SiO$_2$ (Fig. 5). The obtained parameters are given in Table II.

The classical scheme defined in this way accounts well for the energetics of an interstitial O$_2$ molecule in $a$-SiO$_2$. For the energies of equilibrium sites used in the fit, the classical scheme reproduces the first principles data within a rms error of about 0.1 eV. Moreover, to verify the reliability of
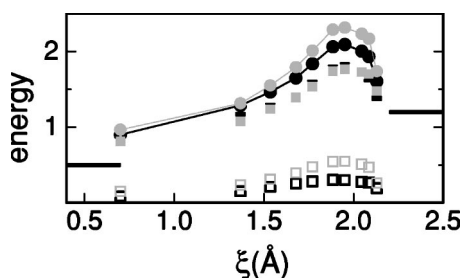
FIG. 7. A comparison between first-principles (black disks) and classical (gray disks) energies in the proximity of the transition state for the $O_2$ migration between two nearest neighbor minima. The thick black lines indicate the energy levels of the two minima, which are separated by a distance of about 3.3 Å. The coordinate $\xi$ specifies the distance of the $O_2$ molecule to the minimum on the left. The energies separate into contributions from the $SiO_2$ relaxation (open squares) and the $O_2$-$SiO_2$ interaction (closed squares).

this simplified scheme for describing transition states, we generate several $O_2$ migration paths within the classical scheme (Sec. III B). For a discrete set of configurations along these pathways, we fully relax the atomic structure by first principles, while keeping fixed the center of mass of the $O_2$ molecule with respect to that of the network. We consider migration pathways with different transition energies. The largest differences between first-principles and classical energies are found for the pathway with the highest transition barrier (2.2 eV). However, even in this case, the errors are always smaller than 0.18 eV as illustrated by the corresponding energy profile in Fig. 7. The difference between first-principles and classical energies raises along the transition path, acquiring its largest value at the transition state (Fig. 7). We note that the error does not derive from the $O_2$-$SiO_2$ interaction, which is overall well described by our modeling scheme, but rather from the relaxation of the $SiO_2$ network which directly results from the adopted interatomic potentials.[67] During the $O_2$ diffusion process, even for transition energies as high as 2.2 eV, the energy along the migration path is dominated by the $O_2$-$SiO_2$ interaction, the $SiO_2$ deformation contributing by at most 20%. This results in an overall error of about 10% for the classical energies with respect to the first-principles ones.

### B. Equilibrium sites, transition barriers, and connections between equilibrium sites

To investigate the potential energy landscape for $O_2$ diffusion in $a$-$SiO_2$, we use the classical scheme (Sec. III A) and span the full volume associated to the set of model structures generated by classical molecular dynamics (Sec. II C). We first search for local minima of the potential energy landscape. We insert the $O_2$ molecule randomly in the model structure of the oxide and adopt a damped molecular dynamics approach for finding the corresponding equilibrium position. For each model structure of $a$-$SiO_2$, the procedure is repeated until convergence on the number of local minima is reached. As a result of the disordered nature of the oxide, the energy distribution of local minima shows a finite spread (Fig. 8). In agreement with the first-principles results ob-
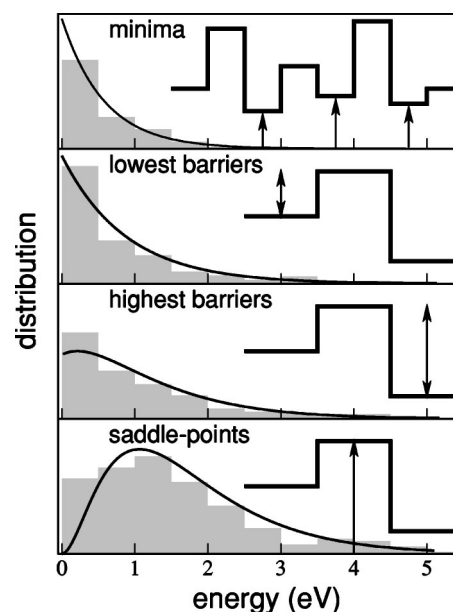


FIG. 8. From top to the bottom, energy distributions of local minima, lowest barriers, highest barriers, and saddle points, for the interstitial $O_2$ molecule in $a$-$SiO_2$. The energy reference is the same as in Fig. 5. Histograms refer to distributions obtained exploring model structures for the oxide within the classical scheme. Exponential decaying functions (solid curves) are found to fit distributions of minima and lowest barriers very well. The continuous distributions for highest barriers and saddle points are obtained by convolving the exponentials for minima and lowest barriers under the assumption of independence, and are found to compare well with the histograms extracted from the actual atomistic model structures.

tained for a limited set of cases (Sec. II D), essentially all these energies remain well below those of network oxygen species. The distribution of $O_2$ minima in $a$-$SiO_2$ is well described by an exponential function with a decay constant of 0.6 eV. The density of equilibrium sites and their average energy are similar for the various model structures of the oxide. This suggests that equilibrium sites are weakly correlated with specific structural features and that they are uniformly distributed in $a$-$SiO_2$.

The equilibrium sites for $O_2$ diffusion allow us to determine the distribution of interstitial volumes available in $a$-$SiO_2$. To each local minimum we associate the largest ellipsoidal volume centered on the $O_2$ molecule and contained in the interstitial void. The resulting distribution of volumes is shown in Fig. 9, and only slightly differs from that obtained through the Voronoi analysis [Fig. 6(b)]. Indeed, from this distribution we find a concentration of local minima for $O_2$ in $a$-$SiO_2$ of $5.4 \times 10^{21}$ cm$^{-3}$, corresponding to an average distance between solubility sites of 5.7 Å. This distance is very close to the value of 4.7 Å, extracted on the basis of simple geometrical criteria from the distribution of Voronoi spheres (Sec. II E). The difference should be attributed to the occurrence of an unphysically large number of small interstitials when adopting the geometrical criteria.

To explore energy barriers between interstitials and accordingly determine the connectivity properties of the disor-
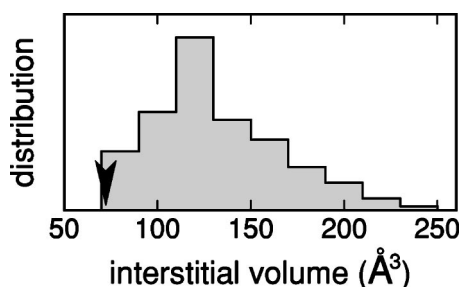
FIG. 9. The distribution of interstitial ellipsoidal volumes for the $O_2$ molecule in $a$-$SiO_2$, as obtained by exploring the model structures of the oxide within the classical scheme. The arrow gives the result for $\alpha$-quartz.



FIG. 10. The distribution of distances between nearest neighbor equilibrium sites for the interstitial $O_2$ molecule in $a$-$SiO_2$.

dered network of local minima, we still adopt the classical scheme described in Sec. III A. We search for saddle points of the potential energy landscape by applying two different methods: the activation relaxation technique (ART)[68] and a dragging procedure.[69] In the ART method, a system is driven from a local minima to a saddle point by partially reversing the restoring force.[68] In our particular case, the transition states can be found by using a reaction coordinate corresponding to the translational motion of the $O_2$ molecule from a particular equilibrium site to a nearest neighboring one. Therefore, we simplify the ART technique reversing only the forces associated to the translational degrees of freedom of the $O_2$ molecule. Furthermore, at variance with respect to the original ART formulation,[68] the coefficient controlling the fraction of the reversed force component is varied during the ART evolution in order to ensure fixed strides of $5 \times 10^{-4}$ Å for the motion of the $O_2$ center of mass. Such a constant slow evolution rate allowed us to construct transitions pathways for the $O_2$ molecule in which the $SiO_2$ network is fully relaxed at each step. For each local minimum, after having randomly displaced the $O_2$ molecule from equilibrium, ART is applied to generate the transition path leading across a saddle point to another nearest neighbor local minimum. This procedure is repeated for each local minimum until convergence on the number of discovered nearest neighbor minima is reached.

To validate this approach, we also determine saddle points and connections using a constrained molecular dynamics technique.[69] For each pair of local minima, the center of mass of the $O_2$ molecule is continuously dragged across the $SiO_2$ network from one local minimum to the other. At each step of the dragging procedure, we reduce the distance between the $O_2$ molecule and the target minimum by $5 \times 10^{-3}$ Å and determine the ground state configuration of the system while the $O_2$-minimum distance is kept fixed. The path through the $SiO_2$ network is interrupted if, during the evolution, the $O_2$ molecule meets another local minimum. The saddle point energies and number of nearest neighbor minima obtained with the two approaches coincide. The results of this investigation are reported in Fig. 8.

Since nonequivalent local minima share asymmetric barriers, we reported separately distributions for lowest and highest barriers. The distribution of the lowest barriers between nearest neighbor minima is well reproduced by an exponential function with a decay constant of 0.9 eV. More-
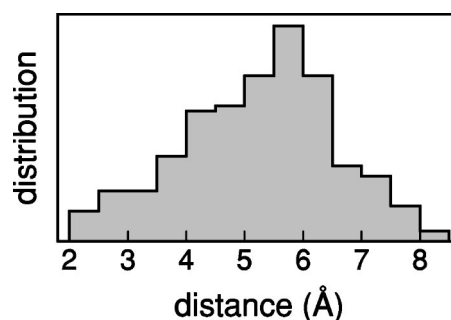
over, from the statistical analysis of our data results that minima and lowest barriers are uncorrelated quantities. In fact, we verified that distributions of highest barriers and saddle points are properly reproduced by convolving the distributions of minima and lowest barriers, as appropriate for independent quantities (Fig. 8). We note that the energy barriers recently calculated in Refs. 29 and 32 are consistent with the barrier distributions shown in Fig. 8.

By identifying the transition states between nearest neighbor local minima, we also access the topological properties of the random network for interstitial $O_2$ diffusion in $a$-$SiO_2$. Indeed, the transition states define the connections between nearest neighbor equilibrium sites. The distribution of distances between such sites is shown in Fig. 10. The average distance derived from this distribution is 5.3 Å, only slightly different from that estimated on the basis of the concentration of energy minima (5.7 Å). Moreover, we extract the connectivity properties of the disordered interstitial network (Fig. 11). The number of connections per node extends from 2 to 6, with an average number of 3.3. For the purpose of further investigation, it is convenient to note that the distribution of connections extracted from the model structures of the oxide is well reproduced by a sixth-degree binomial distribution with coefficient 0.55.

### C. $O_2$ solubility in $a$-$SiO_2$

We here provide an estimate of the $O_2$ solubility in $a$-$SiO_2$ on the basis of the information acquired on its equi-
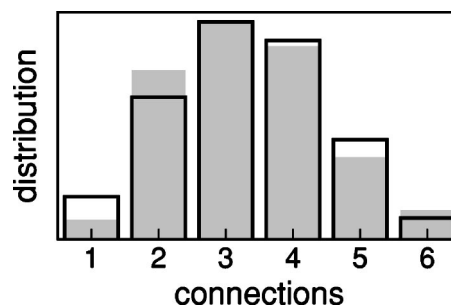


FIG. 11. The distribution of connections between nearest neighbor equilibrium sites in amorphous $SiO_2$ at regular density. A sixth-degree binomial distribution with a coefficient of 0.55 (open histogram) is found to well reproduce the data extracted from the atomistic model structures of the oxide (filled histogram).

librium sites. We suppose that a *gas* of independent $O_2$ molecules dissolved in the interstitials of $a$-$SiO_2$ is in equilibrium with a gas of free molecules. Thus, according to classical thermodynamics,[70–72] the chemical potential ($\mu$) for $O_2$ is the same both in vacuum and in $SiO_2$. Hence $\mu_{\text{free}} = \mu_{SiO_2}$ or, equivalently,

$$-k_B T \ln\left(\frac{\mathcal{Z}_{\text{free}}}{N_{\text{free}}}\right) = -k_B T \ln\left(\frac{\mathcal{Z}_{SiO_2}}{N_{SiO_2}}\right), \qquad (2)$$

where $\mathcal{Z}_{\text{free}}$, $N_{\text{free}}$ and $\mathcal{Z}_{SiO_2}$, $N_{SiO_2}$ are the partition function and the number of $O_2$ molecules in vacuum and $a$-$SiO_2$, respectively. $T$ is the temperature and $k_B$ the Boltzmann constant.

Accounting for the distribution of interstitials in $a$-$SiO_2$ available for the $O_2$ molecule (Fig. 9), we can write $\mathcal{Z}_{SiO_2}$ as follows:

$$\mathcal{Z}_{SiO_2} = V_{SiO_2} \mathcal{N}_{SiO_2} \int m(E) \mathcal{Z}_{V(E)} dE, \qquad (3)$$

where $V_{SiO_2}$ and $\mathcal{N}_{SiO_2}$ are the volume of the oxide and the concentration of solubility sites for $O_2$, respectively. $m(E)$ corresponds to the energy distribution of local minima for $O_2$ in the oxide (Fig. 8, top panel), whereas $\mathcal{Z}_{V(E)}$ is the partition function for the molecule in $a$-$SiO_2$ where the spatial integration is limited to the volume $V(E)$ associated to the equilibrium site of energy $E$.

Evaluating Eq. (3) to obtain the solubility $n_{SiO_2}$ ($n_{SiO_2} = N_{SiO_2}/V_{SiO_2}$) through Eq. (2) is a complicated task.[72] By assuming a uniform distribution of identical solubility sites, early investigations estimated the binding energy of rare gases and inert molecules in $a$-$SiO_2$ by direct comparison with solubility data.[73,74] More recently, Monte-Carlo simulations based on interatomic potentials addressed the calculation of Eq. (3) for rare gases dissolved in $a$-$SiO_2$ obtaining a qualitative agreement with experiments.[71]

Here, we estimate the $O_2$ solubility in the oxide on the basis of crude approximations.[72] In particular, we assume that a $O_2$ molecule in the oxide can access only a limited region of space in the neighborhood of each equilibrium site. These spatial regions constitute a network of physically separated volumes in which the $O_2$ molecule is completely free to move, rotate and vibrate, as in vacuum. The surrounding oxide determines the energy $E$ with respect to vacuum. Adopting this picture and using the partition function for an ideal gas composed of $N_{\text{free}}$ oxygen molecules at a temperature $T$ and pressure $p$, from Eq. (3) we obtain

$$n_{SiO_2} = \frac{p}{k_B T} \mathcal{N}_{SiO_2} \int m(E) V(E) \exp\left(-\frac{E}{k_B T}\right) dE. \qquad (4)$$

To evaluate the solubility $n_{SiO_2}$ by using Eq. (4), we consider the energies of the equilibrium sites in our set of model structures of $a$-$SiO_2$ (Fig. 8). For each energy minimum, we then define the associated spatial region as the sphere centered on the equilibrium site and with radius half the distance to the next-nearest neighbor $O_2$ equilibrium site. For a pressure of 1 atm and a temperature of 1078 °C, we obtain in this way a solubility of $n_{SiO_2} = 19.4 \times 10^{16}$ cm$^{-3}$, to be com-

pared with the corresponding experimental value of 5.5 $\times 10^{16}$ cm$^{-3}$.[9] This comparison between theory and experiment should be considered very satisfactory. Indeed, the observed difference for the solubility corresponds to an error of about 0.1 eV on the energy scale of the energy minima for the $O_2$ molecule in $a$-$SiO_2$, within the uncertainty of our level of theory.

## IV. LONG-RANGE $O_2$ DIFFUSION IN SILICA

The average energy barrier between neighboring local minima for $O_2$ in $a$-$SiO_2$ is about 0.7 eV. This value is sufficiently high for assuming that dynamical correlation effects, such as recrossing events or consecutive multiple jumps, are negligibly small during diffusion.[75] Under this assumption, the transition-state theory, which defines transition rates according to the relative energy position of minima and saddle points,[76] constitutes a suitable approach for studying the diffusion process. In this framework, the statistical properties of the $O_2$ energy landscape (Fig. 8) and of the topology of the interstitial network (Fig. 11) are relevant ingredients for studying the diffusion process.

### A. Random lattice model

To model in a statistical meaningful way the long-range diffusion process, it is necessary to further increase the length and time scales spanned in our investigation. Therefore, we turn to a lattice model with the intent of preserving (i) the nearest-neighbor connectivity and (ii) the energy distributions of minima and saddle points, found within our classical modeling scheme. We consider a cubic lattice model, in which each site mimics an equilibrium position in an interstitial void of $a$-$SiO_2$ and each bond between nearest neighbor lattice sites represents the transition path between two nearest neighbor equilibrium sites. We find that a lattice model of $30 \times 30 \times 30$ is sufficiently large to model the diffusion properties. Since the average distance between nearest-neighbor equilibrium sites is of 5.3 Å (Fig. 10), this lattice model corresponds to a cubic sample of $a$-$SiO_2$ with a side of 17 nm.

The distribution of connections between nearest neighbor local minima is well reproduced by the binomial function

$$\mathcal{B}_N^p(n) = \frac{N!}{n!\,(N-n)!} p^n (1-p)^{N-n}, \; n = 1, \dots N, \qquad (5)$$

with $N = 6$ and $p = 0.55$. Hence, to reproduce the connectivity of the network of interstitials for the $O_2$ molecule in $a$-$SiO_2$, we choose a fraction $1 - p = 0.45$ of the bonds at random and omit them from the outset (infinite energy barrier). To the remaining bonds, we assign finite energy barriers according to the distributions found for our atomistic model structures of the disordered oxide (Fig. 8). For simplicity, we make use of the continuous exponential distributions. This random assignment of energies and connections is expected to accurately mimic the actual interstitial network, in view of the weak correlations observed in the atomistic model structures.

## B. Monte-Carlo simulations

According to the transition-state theory,[76] transition rates for hopping between nearest neighbor equilibrium sites are defined by energy barriers and attempt frequencies. The diffusion coefficient is then determined by the geometrical properties of the disordered network hosting the migration process, namely the distributions of distances and connections between nearest-neighbor equilibrium sites.[75] For distributions of energies, attempt frequencies, connections, and distances showing finite first and second moments, the diffusion process is normal.[77,78] Under these conditions, distances between nearest neighbor sites and hopping attempt frequencies influence the absolute value of the diffusion coefficient, whereas the energetical and topological properties of the disordered network determine its dependence on temperature.[77,78]

In our Monte-Carlo simulations, the attempt frequencies, or equivalently the rattling times within the interstitial volumes, are assumed to be identical and independent of the energy of the equilibrium site. Since the $O_2$ molecule visits interstitials covering a limited range of energies during diffusion (see Sec. IV C), this assumption appears reasonable. The distribution of distances between nearest-neighbor equilibrium sites is well localized around a mean value of 5.3 Å (Fig. 10). Therefore, distances between nearest neighboring sites are supposed to be the same in our simulations. Our principal goal is the calculation of the effective activation energy for diffusion, a quantity which is strictly related to the energetical and topological properties of the potential energy landscape.

To find the effective activation energy for $O_2$ diffusion in the oxide, we distribute a set of 1000 independent moving particles ($O_2$ molecules) on the random lattice model (disordered network of interstitials in $a$-SiO$_2$). The particles are then evolved at a specified temperature by adopting the Metropolis Monte-Carlo algorithm.[79] In particular, at each Monte-Carlo step, for a specified diffusing particle at the lattice site $i$, a transition path toward another nearest neighboring equilibrium site $j$ is chosen at random and the particle is transferred to $j$ according to the probability $\exp[-E_b(i \rightarrow j)/k_B T]$, where $T$ is the temperature and $E_b(i \rightarrow j)$ the energy barrier associated to the transition $i \rightarrow j$.

At low temperature, the diffusion coefficient obtained by the Monte-Carlo simulations converges slowly.[80] To increase the efficiency of the scheme, we therefore adopt a modified version of the Metropolis algorithm.[80] The acceleration of the scheme is achieved by raising the energy values of all minima by a small amount $\epsilon$ or, equivalently, by augmenting the hopping rates by a factor $\mathcal{A} = \exp(\epsilon/kT)$. To preserve the absolute values for transition rates, the time unit is also scaled by the acceleration factor $\mathcal{A}$. Neither the equilibrium distribution of particles in the local minima nor the relative transition rates between nearest neighbor sites are altered by this modification. Furthermore, by adopting small values for $\epsilon$, the particle dynamics is altered only at short times because of the modified energy landscape. The long-range diffusion properties are determined by energy barriers greater than $\epsilon$ and are therefore preserved.[80] We successfully determine diffusion coefficients using $\epsilon = 0.17$ eV.
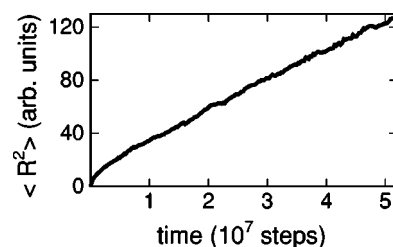


FIG. 12. Average mean square displacement of the diffusing particles vs. time at 1200 K. The time step used in the simulation corresponds to an arbitrary unit.

## C. Activation energy for $O_2$ diffusion in $a$-SiO$_2$

During the Monte-Carlo simulations on random lattice models, the average mean-square displacement follows a normal diffusive behavior,[77] increasing linearly with time after an initial sublinear regime (Fig. 12). Thus, from each Monte-Carlo simulation, we derive a diffusion coefficient using Einstein's relation.[77] At every considered temperature, several Monte-Carlo simulations are performed for different configurations of the random lattice. The averaged results are reported in Fig. 13.

Diffusion coefficients are estimated at temperatures ranging from 1000 K to 1500 K, which correspond to typical temperatures adopted during silicon oxidation. In this interval of temperatures, the $O_2$ diffusion coefficient follows a quasi-Arrhenian behavior with a corresponding effective activation energy of 1.12 eV (Fig. 13). The calculated activation energy is in excellent agreement with experimental values obtained at similar temperatures (1.04–1.26 eV).[9,81–83]

During the Monte-Carlo evolution, the diffusing particles visit a particular distribution of minima and saddle points of the disordered energy landscape.[33] Visited minima are concentrated at the lowest energy values for $O_2$ in $a$-SiO$_2$. The energy distribution of the visited saddle points is broader. When the energies are referenced with respect to the most stable minimum in SiO$_2$, the highest energy values visited during the motion are located around the effective activation energy for $O_2$ diffusion.[33] The highest energy level reached during the diffusion process remains well below the energy intervals corresponding to peroxyl and ozonyl linkages (Fig. 5), indicating that network oxygen exchange processes are unlikely during $O_2$ diffusion. This result is consistent with experimental observations which found evidence for such
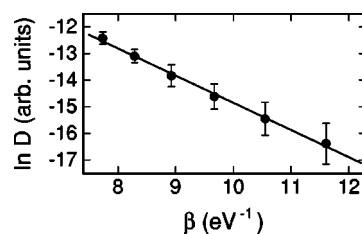


FIG. 13. Logarithm of the diffusion coefficient extracted from Monte-Carlo simulations at different temperatures ($\beta = 1/k_B T$). Each of the diffusion coefficients (disks) is obtained as an average over eight simulations. The error bars are the relative rms deviations.

exchange processes only at the SiO$_2$ surface and at the Si-SiO$_2$ interface, but not in the bulk of the SiO$_2$ layer.[11–15,17,18]

These results highlight the percolative nature of the O$_2$ diffusion process in the disordered oxide. The long-range diffusion mainly involves the lowest-energy part of the energy landscape still allowing for percolation throughout the oxide. In Ref. 33, we showed that the activation energy for the long-range diffusion results from the combination of both the energetical and topological properties of the O$_2$ energy landscape in $a$-SiO$_2$.

## V. DEPENDENCE OF THE O$_2$ DIFFUSION RATE ON OXIDE THICKNESS

In the Deal and Grove model,[5] the inverse growth rate, $1/R$, depends on the oxide thickness $X$ as follows:

$$\frac{1}{R} = \frac{1}{k_l} + \frac{2X}{k_p}, \qquad (6)$$

where the linear ($k_l$) and parabolic ($k_p$) constants are proportional to the O$_2$ interfacial oxidation reaction rate and the O$_2$ diffusivity in the oxide, respectively.[7,85] Equation (6) well describes the growth rates when the oxide film is sufficiently thick ($\geq 20$ nm).[5] However, for very thin oxide films, the rate given by Eq. (6) significantly deviates from experimental values.[7,85] Indeed, in this regime, the experimental growth rates appear anomalously larger than $k_l$, the value predicted by the Deal and Grove model for $X \sim 0$ [cf. Eq. (6)].[84,85] Many interpretations have been put forward to describe this behavior.[84,85,8] The most accredited among them assumes that the oxidation kinetics depends only on the diffusion of the oxidizing species ($k_l \rightarrow \infty$), with a variable diffusion rate across the oxide layer.[84–86] In particular, to reproduce the experimental growth rates the diffusion rate should decrease as the oxide film becomes thinner. As a matter of fact, this assumption is currently adopted in modern models which successfully account for the silicon oxidation kinetics in both the thin and the thick oxide regimes.[87] However, an atomic scale description of the diffusion rate corroborating this behavior is lacking.

The O$_2$ diffusion rate through a thin oxide film ($<20$ nm) with the same properties and density as $a$-SiO$_2$ is expected to increase significantly because of the percolative nature of the diffusion mechanism.[87,33] In fact, on a short-range scale, $a$-SiO$_2$ is not homogeneous and the diffusion rate increases due to the occurrence of small-barrier pathways. This effect is in clear contrast with experimental observations. Another mechanism is therefore expected to oppose this behavior leading to an overall lower diffusivity with respect to the bulk. Such an opposing effect might be achieved by the presence of an oxide layer of higher density in the neighborhood of the silicon substrate, as revealed by x-ray reflectivity experiments.[34,35] Indeed, this layer is expected to reduce the diffusivity.[88]

In this section, we specifically focus on the effect of an interfacial oxide layer of higher density on the O$_2$ diffusion rate across the thin oxide. We note that, although other mechanisms might be operative in the thin oxide regime,[89,29] we assume here that the interstitial O$_2$ molecule dominates the oxygen diffusion process across the film, regardless of its thickness.

### A. O$_2$ diffusion in amorphous SiO$_2$ of higher density

We describe amorphous SiO$_2$ of higher density ($d$-SiO$_2$) by a set of atomistic model structures, generated by classical molecular dynamics.[54,55] We use periodically repeated cubic cells of fixed volume, corresponding to a density of 2.4 g/cm$^3$, as estimated by x-ray reflectivity measurements for the oxide in the vicinity of the Si-SiO$_2$ interface.[34,35] To generate model structures, we adopt the procedure described in Sec. II C. We construct 16 model structures with a number of atoms in the periodic cell ranging between 72 and 90. All the model structures consist of random networks of corner-sharing tetrahedral SiO$_4$ units, without any coordination defect. As compared with $a$-SiO$_2$ at the regular density, structural parameters are only slightly affected by the increased density (Table I). The reduced volume per SiO$_2$ unit appears to be accommodated by the reduction of the mean Si-O-Si bond angle and consequently of the distance between Si atoms in neighboring tetrahedral units. The increased density also barely affects the ring statistics (Fig. 4). In fact, as compared with $a$-SiO$_2$ at the regular density (cf. Sec. II C), the model structures of $d$-SiO$_2$ only show a small decrease of the threefold rings in favor of sixfold rings. The calculated structure factor compares well with experimental data and correctly shows a shift of the first sharp diffraction peak toward a value of about 1.7 Å$^{-1}$.[90] This agreement indicates that the intermediate range order in our model structures is properly described.

We explore the potential energy landscape for the interstitial O$_2$ molecule in $d$-SiO$_2$ following the same procedure as in the case of $a$-SiO$_2$ (cf. Sec. III). We use the extended set of model structures generated for the oxide of higher density and describe the energetics with the classical scheme given in Sec. III A. We first search for equilibrium sites of interstitial O$_2$ molecules in $d$-SiO$_2$. We find a concentration of local minima of $6.7 \times 10^{21}$ cm$^{-3}$ and an average distance of about 5.3 Å between nearest neighbor minima. These values are very close to those found for amorphous SiO$_2$ at regular density ($5.4 \times 10^{21}$ cm$^{-3}$, 5.7 Å). On the other hand, the energy distribution of local minima undergoes important changes. In particular, the mean value of this distribution shifts to a higher energy by 0.6 eV with respect to the mean value for amorphous SiO$_2$ at regular density (Fig. 14). This property is consistent with the decrease of the average interstitial volume in $d$-SiO$_2$. In fact, the O$_2$-network energy increases for decreasing interstitial volumes (cf. Fig. 5).

We then locate the saddle points of the potential energy landscape and their corresponding energies. The transition states connect neighboring minima by an asymmetric barrier. The energy barrier distribution associated to the low barrier side is well described by an exponential function with a decay constant of 1.7 eV (Fig. 14). This should be compared with the corresponding value of 0.9 eV for $a$-SiO$_2$. These results indicate that the potential energy landscape for O$_2$
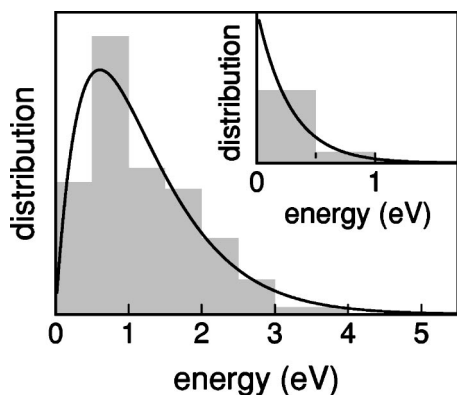
FIG. 14. Energy distributions of minima and lowest barriers (inset) for diffusion of the interstitial $O_2$ molecule in amorphous $SiO_2$ at a density of 2.4 g/cm$^3$. Histograms refer to distributions obtained exploring actual model structures of the oxide, while solid lines correspond to fitted continuous distributions.

diffusion in $d$-$SiO_2$ is considerably shifted toward higher energies as compared to amorphous $SiO_2$ at regular density.

The location of the transition states defines an interstitial network for $O_2$ diffusion. The local minima form the nodes of this network. Our analysis shows that in $d$-$SiO_2$ the number of connections per node can vary between one and 10. The average number of connections per node is found to be 4.1 (Fig. 15). The associated distribution can be well reproduced by a binomial distribution, characterized by parameters $N=12$ and $p=0.34$.

To study the $O_2$ diffusion in $d$-$SiO_2$, we use a periodic fcc lattice model with $50 \times 50 \times 50$ independent sites. For a mean distance between local minima of 5.3 Å, this corresponds to a cubic volume of side $\sim 19$ nm. Assuming that neighboring nodes and barriers are uncorrelated, we transfer the nearest neighbor connectivity and the energy distributions derived from the atomistic structural models onto the lattice model. Monte-Carlo simulations for 2000 diffusing particles were performed at temperatures ranging between 1000 K and 1500 K. Minima and saddle points visited during the diffusion fall below the energies of competitive oxygen species, thereby indicating that the interstitial $O_2$ molecule remains the favorite transported oxygen species also in amorphous $SiO_2$ with a density 2.4 g/cm$^3$. The calculated
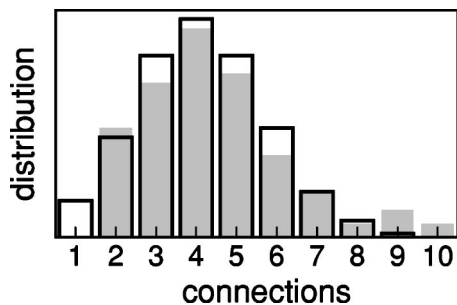


FIG. 15. Distribution of connections between nearest neighbor equilibrium sites in amorphous $SiO_2$ at a density of 2.4 g/cm$^3$. A twelfth-degree binomial distribution with a coefficient of 0.34 (open histogram) is found to well reproduce the data extracted from atomistic model structures representing this oxide (filled histogram).
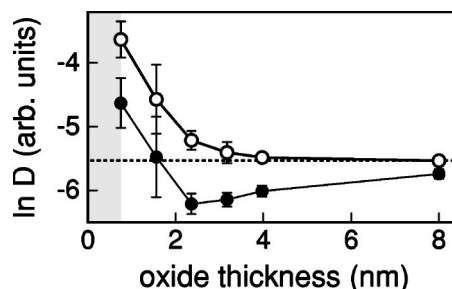


FIG. 16. Calculated diffusion coefficients in the direction perpendicular to the plane of the interface for homogeneous (open symbols) and nonhomogeneous (closed symbols) oxide layers of varying thickness at Si-$SiO_2$ interfaces. The horizontal dashed line corresponds to the diffusion coefficient in bulk $SiO_2$. The shaded region indicates the thickness of the interfacial oxide layer of higher density (2.4 g/cm$^3$), considered in our simulations of the nonhomogeneous oxide layer.

diffusion coefficients are interpolated by an Arrhenius law with an effective activation energy of 2.0 eV, consistent with the experimental estimate of 2.0-2.4 eV for $O_2$ diffusion in an amorphous $SiO_2$ sample with a density of about 2.5 g/cm$^3$.[88]

### B. $O_2$ diffusion through the oxide layer at the Si-$SiO_2$ interface

To model the $O_2$ diffusion through oxide layers of different thickness, we perform Monte-Carlo simulations on periodic lattice models of variable size in the direction $z$. In particular, we consider fcc lattice models of $50 \times 50 \times N$ sites, where $N$ is varied from 2 to 20, corresponding to oxide thicknesses between 1 and 10 nm. The reduced periodicity in the $z$ direction effectively models the diffusion in a thin oxide layer, as occurs at the Si-$SiO_2$ interface. In the other directions ($x$ and $y$), the system is sufficiently large to recover the bulk limit. The diffusion coefficient is calculated at 1300 K, a temperature typically adopted for the thermal oxidation of silicon.

At first, we consider the case of homogeneous oxide layers. We assign energies and connections to the lattice model according to distributions extracted for amorphous $SiO_2$ at regular density. In particular, a good representation of the nearest-neighbor connectivity on the fcc lattice is obtained for a binomial function with $p=0.27$. The results of the Monte-Carlo simulations show that the rate for diffusion along $z$ increases for decreasing oxide thickness (Fig. 16). This behavior can be understood in terms of the percolative nature of the diffusion process. In fact, when the layer thickness drops, the number of low-barrier paths increases, resulting in an increase of the diffusion coefficient. For thick layers, the bulk value is recovered. We note that an increase of the diffusion coefficient for thin oxide layers *cannot* explain the anomalous deviations from the Deal-Grove model in the initial stages of oxidation.[91,85]

X-ray reflectivity experiments indicate the occurrence of a 10-Å-thick oxide layer of higher density (2.4 g/cm$^3$) in the proximity of the Si-$SiO_2$ interface.[34,35] We model the pres-

ence of this dense layer by including in our lattice models two planes, on which we map connectivity and energetic properties corresponding to amorphous $SiO_2$ with a density of 2.4 g/cm$^3$ (Fig. 15). For the remaining $N-2$ planes, we use the properties appropriate for amorphous $SiO_2$ at regular density. The two layers are separated by two planes of interlayer connections. For one plane of such connections, we use properties of amorphous $SiO_2$ at regular density and for the other those of $SiO_2$ at higher density.

The diffusion coefficient for such oxide layers is given as a function of oxide thickness in Fig. 16. As expected, the diffusion coefficient is now lower than for homogeneous oxide layers. More interestingly, the diffusion coefficient falls below the bulk limit for oxide thicknesses down to about 2 nm. This result indicates that the presence of a denser oxide can indeed account for a lower diffusion coefficient during oxidation. The diffusion coefficient is found to vary as a function of oxide thickness, approaching from below the bulk limit corresponding to amorphous $SiO_2$ at regular density. As long as the diffusion coefficient significantly differs from the bulk limit, deviations with respect to the Deal-Grove oxidation kinetics can be expected. This behavior of the diffusion coefficient as a function of oxide thickness is in qualitative agreement with experimental data for the oxidation kinetics.[8]

For oxide thicknesses below 2 nm, size effects due to percolation still dominate the diffusion coefficient in our model oxide layers. However, in these early stages of oxidation, the specific bonding pattern at the interface as well as the occurrence of other atomic scale processes might invalidate the underlying assumptions of our approach. Such processes include diffusion of peroxy linkages and charged species, exchange processes between gas-phase and network oxygen atoms.[89,29]

## VI. CONCLUSION

The present work provides an atomistic picture for the oxygen diffusion mechanism during silicon oxidation in the thick oxide regime. We first focus on the diffusion process occurring in a region far from the Si(100)-$SiO_2$ interface, where the oxide properties correspond to those of amorphous $SiO_2$. We identify the interstitial $O_2$ molecule as the diffusing species in $a$-$SiO_2$. We provide a statistical characterization of the disordered network of interstices for $O_2$ diffusion in $a$-$SiO_2$ in terms of distributions of energy minima, transition barriers and number of connections between nearest neighbor minima. Then, we address the long-range diffusion process by mapping these distributions on an extended lattice model and using a Monte-Carlo approach. We find an activation energy for diffusion of 1.12 eV, in excellent agreement with experimental data.[9,81–83] Furthermore, our study highlights the percolative nature of the diffusion process and the critical dependence of the diffusion rate on both the energetical and topological properties of the interstitial network.[33]

Next, we address the $O_2$ diffusion rate through the oxide layer at Si(100)-$SiO_2$ interfaces focusing on the effect of a dense oxide layer located close to the silicon substrate. We first extend our atomic-scale description of $O_2$ diffusion in amorphous $SiO_2$ to the case of an oxide of higher density (2.4 g/cm$^{-3}$). This yields an activation energy of 2.0 eV which compares well with the experimental result.[88] Then, we investigate the dependence of the $O_2$ diffusion rate on oxide thickness at Si(100)-$SiO_2$ interfaces using Monte-Carlo simulations. We consider both homogeneous and nonhomogeneous oxide layers. The nonhomogeneous oxide is composed of two layers: one at regular density and one at higher density. The thickness and the mass density of the denser layer are taken from x-ray reflectivity measurements.[34,35] In the case of a regular oxide, we find that the $O_2$ diffusion rate increases for decreasing thickness, as a result of the percolative nature of the diffusion mechanism. When the occurrence of an oxide layer of higher density is considered, the diffusion coefficient drops below its value for bulk $a$-$SiO_2$, for oxide thicknesses larger than 2 nm. This result is consistent with the observed oxidation kinetics.[8]

*Present address: Georgia Institute of Technology, School of Physics, 837 State Street, Atlanta, Georgia 30332-0430, USA.

[1] L. C. Feldman, E. P. Gusev, and E. Garfunkel, in *Fundamental Aspects of Ultrathin Dielectrics on Si-based Devices*, edited by E. Garfunkel *et al.* (Kluwer, Dordrecht, 1998), pp. 1–24.

[2] D. A. Muller, S. Moccio, F. H. Baumann, K. Evans-Lutterodt, and G. Timp, Nature (London) **399**, 758 (1999).

[3] M. L. Green, E. P. Gusev, R. Degraeve, and E. L. Garfunkel, J. Appl. Phys. **90**, 2057 (2001).

[4] M. Schulz, Nature (London) **399**, 729 (1999).

[5] B. E. Deal and A. S. Grove, J. Appl. Phys. **36**, 3770 (1965).

[6] R. Ghez and Y. J. van der Meulen, J. Electrochem. Soc. **119**, 1100 (1972).

[7] M. A. Hopper, R. A. Clarke, and L. Young, J. Electrochem. Soc. **122**, 1216 (1975).

[8] H. Z. Massoud, J. D. Plummer, and E. A. Irene, J. Electrochem. Soc. **132**, 1745 (1985).

[9] F. J. Norton, Nature (London) **191**, 701 (1961).

[10] W. G. Perkins and D. R. Begal, J. Chem. Phys. **54**, 1683 (1971).

[11] E. Rosencher, A. Straboni, S. Rigo, and G. Amsel, Appl. Phys. Lett. **34**, 254 (1979).

[12] F. Rochet, B. Agius, and S. Rigo, J. Electrochem. Soc. **131**, 914 (1984).

[13] F. Rochet, S. Rigo, M. Froment, C. d'Anterroches, C. Maillot, H. Roulet, and G. Dufour, Adv. Phys. **35**, 237 (1986).

[14] I. Trimaille and S. Rigo, Appl. Surf. Sci. **39**, 65 (1989).

[15] J. A. Costello and R. E. Tressler, J. Electrochem. Soc. **131**, 1944 (1984).

[16] E. P. Gusev, H. C. Lu, T. Gustafsson, and E. Garfunkel, Phys. Rev. B **52**, 1759 (1995).

[17] T. Åkermark, L. G. Gosset, J.-J. Ganem, I. Trimaille, and S. Rigo, J. Electrochem. Soc. **146**, 3389 (1999).

[18] T. Åkermark, J.-J. Ganem, I. Trimaille, I. Vickridge, and S. Rigo, J. Phys. Chem. B **103**, 9910 (1999).

[19] T. Åkermark, J. Electrochem. Soc. **147**, 1882 (2000).

[20] N. F. Mott, Philos. Mag. A **45**, 323 (1982).

[21] N. F. Mott, Philos. Mag. B **55**, 117 (1987).

[22] A. G. Revesz and H. A. Schaeffer, J. Electrochem. Soc. **129**, 357 (1982).

[23] D. R. Hamann, Phys. Rev. Lett. **81**, 3447 (1998).

[24] M. A. Szymanski, A. M. Stoneham, and A. L. Shluger, Microelectron. Reliab. **40**, 567 (2000).

[25] J. R. Chelikowsky, D. J. Chadi, and N. Binggeli, Phys. Rev. B **62**, R2251 (2000).

[26] G. Roma, Y. Limoge, and S. Baroni, Phys. Rev. Lett. **86**, 4564 (2001).

[27] W. Orellana, A. J. R. da Silva, and A. Fazzio, Phys. Rev. Lett. **87**, 155901 (2001).

[28] M. A. Szymanski, A. L. Shluger, and A. M. Stoneham, Phys. Rev. B **63**, 224207 (2001).

[29] A. M. Stoneham, M. A. Szymanski, and A. L. Shluger, Phys. Rev. B **63**, 241304(R) (2001).

[30] A. Bongiorno and A. Pasquarello, Microelectron. Eng. **59**, 167 (2001).

[31] Y. Jin and K. J. Chang, Phys. Rev. Lett. **86**, 1793 (2001).

[32] T. Bakos, S. N. Rashkeev, and S. T. Pantelides, Phys. Rev. Lett. **88**, 055508 (2002).

[33] A. Bongiorno and A. Pasquarello, Phys. Rev. Lett. **88**, 125901 (2002).

[34] N. Awaji, S. Ohkubo, T. Nakanishi, Y. Sugita, K. Takasaki, and S. Komiya, Jpn. J. Appl. Phys. **35**, L67 (1996).

[35] S. D. Kosowsky, P. S. Pershan, K. S. Krish, J. Bevk, M. L. Green, D. Brasen, L. C. Feldman, and P. K. Roy, Appl. Phys. Lett. **70**, 3119 (1997).

[36] V. V. Afanas'ev, Microelectron. Eng. **48**, 241 (1999).

[37] P. J. Jorgensen, J. Chem. Phys. **37**, 874 (1962).

[38] D. O. Raleigh, J. Electrochem. Soc. **113**, 782 (1966).

[39] P. J. Jorgensen, J. Electrochem. Soc. **114**, 820 (1967).

[40] D. O. Raleigh, J. Electrochem. Soc. **115**, 111 (1968).

[41] D. N. Modlin and W. A. Tiller, J. Electrochem. Soc. **132**, 1659 (1985).

[42] P. Hohenberg and W. Kohn, Phys. Rev. **136**, B864 (1964).

[43] W. Kohn and L. J. Sham, Phys. Rev. **140**, A1133 (1965).

[44] D. R. Hamann, Phys. Rev. Lett. **76**, 660 (1996).

[45] J. P. Perdew, J. A. Chevary, S. H. Vosko, K. A. Jackson, M. R. Pederson, D. J. Singh, and Carlos Fiolhais, Phys. Rev. B **46**, 6671 (1992).

[46] A. Dal Corso, A. Pasquarello, A. Baldereschi, and R. Car, Phys. Rev. B **53**, 1180 (1996).

[47] D. Vanderbilt, Phys. Rev. B **41**, 7892 (1990).

[48] A. Pasquarello, K. Laasonen, R. Car, C. Lee, and D. Vanderbilt, Phys. Rev. Lett. **69**, 1982 (1992).

[49] K. Laasonen, A. Pasquarello, R. Car, C. Lee, and D. Vanderbilt, Phys. Rev. B **47**, 10 142 (1993).

[50] R. Car and M. Parrinello, Phys. Rev. Lett. **55**, 2471 (1985).

[51] K. Kato, T. Uda, and K. Terakura, Phys. Rev. Lett. **80**, 2000 (1998).

[52] *CRC Handbook of Chemistry and Physics*, edited by D. R. Lide and H. P. R. Frederikse (CRC Press, New York, 1998).

[53] Andrea Trave, Ph.D. thesis, Geneva, 2001.

[54] B. W. H. van Beest, G. J. Kramer, and R. A. van Santen, Phys. Rev. Lett. **64**, 1955 (1990).

[55] K. Vollmayr, W. Kob, and K. Binder, Phys. Rev. B **54**, 15 808 (1996).

[56] R. L. Mozzi and B. E. Warren, J. Appl. Crystallogr. **2**, 164 (1969).

[57] F. Mauri, A. Pasquarello, B. G. Pfrommer, Y. G. Yoon, and S. G. Louie, Phys. Rev. B **62**, R4786 (2000).

[58] S. Susman, K. J. Volin, D. L. Price, M. Grimsditch, J. P. Rino, R. K. Kalia, P. Vashishta, G. Gwanmesia, Y. Wang, and R. C. Liebermann, Phys. Rev. B **43**, 1194 (1991).

[59] S. V. King, Nature (London) **213**, 1112 (1967).

[60] J. P. Rino, I. Ebbsjö, R. K. Kalia, A. Nakano, and P. Vashishta, Phys. Rev. B **47**, 3053 (1993).

[61] P. Umari, X. Gonze, and A. Pasquarello, Phys. Rev. Lett. **90**, 027401 (2003).

[62] J. Sarnthein, A. Pasquarello, and R. Car, Phys. Rev. Lett. **74**, 4682 (1995).

[63] J. Sarnthein, A. Pasquarello, and R. Car, Phys. Rev. B **52**, 12 690 (1995).

[64] V. A. Luchnikov, N. N. Medvedev, A. Appelhagen, and A. Geiger, Mol. Phys. **88**, 1337 (1996).

[65] M. Wilson and P. A. Madden, Phys. Rev. Lett. **80**, 532 (1998).

[66] C. Massobrio and A. Pasquarello, J. Chem. Phys. **114**, 7976 (2001).

[67] For a more detailed comparison between vibrational energies of $SiO_2$ as given by first-principles and by the classical potentials of Ref. 54, we refer the reader to M. Benoit and W. Kob, Europhys. Lett. **60**, 269 (2002).

[68] G. T. Barkema and N. Mousseau, Phys. Rev. Lett. **77**, 4358 (1996).

[69] M. J. S. Dewar, E. F. Healy, and J. J. P. Stewart, J. Chem. Soc., Faraday Trans. **80**, 227 (1984).

[70] Federick Reif, in *Fundamentals of Statistical and Thermal Physics*, edited by E. U. Condon (McGraw-Hill, Singapore, 1965).

[71] B. Guillot and Y. Guissani, J. Chem. Phys. **105**, 255 (1996).

[72] R. Kirchheim, J. Am. Ceram. Soc. **84**, 2699 (2001).

[73] P. L. Studt, J. F. Shackelford, and R. M. Fulrath, J. Appl. Phys. **41**, 2777 (1970).

[74] J. F. Shackelford, P. L. Studt, and R. M. Fulrath, J. Appl. Phys. **43**, 1619 (1972).

[75] A. F. Voter, Phys. Rev. Lett. **63**, 167 (1989).

[76] G. H. Vineyard, J. Phys. Chem. Solids **3**, 121 (1957).

[77] J. W. Haus and K. W. Kehr, Phys. Rep. **150**, 263 (1987).

[78] J-.P Bouchaud and A. Georges, Phys. Rep. **195**, 27 (1990).

[79] N. Metropolis, A. W. Rosenbluth, M. N. Rosenbluth, A. H. Teller, and E. Teller, J. Chem. Phys. **21**, 1087 (1953).

[80] B. Roling, Phys. Rev. B **61**, 5993 (2000).

[81] E. L. Williams, J. Am. Ceram. Soc. **48**, 190 (1965).

[82] H. A. Schaeffer, J. Non-Cryst. Solids **38**, 545 (1980).

[83] M. A. Lamkin and F. L. Riley, J. Eur. Ceram. Soc. **10**, 347 (1992).

[84] A. Fargeix, G. Ghibaudo, and G. Kamarinos, J. Appl. Phys. **54**, 2878 (1983).

[85] N. F. Mott, S. Rigo, F. Rochet, and A. M. Stoneham, Philos. Mag. B **60**, 189 (1989).

[86] R. H. Doremus and A. Szewczyk, J. Mater. Sci. **22**, 2887 (1987).

[87] L. Verdi, A. Miotello, and R. Kelly, Thin Solid Films **241**, 383 (1994); L. Verdi and A. Miotello, Phys. Rev. B **51**, 5469 (1995).

[88] R. A. B. Devine, J. J. Capponi, and J. Arndt, Phys. Rev. B **35**, 770 (1987).

[89] J.-J. Ganem, I. Trimaille, P. Andrè, S. Rigo, F. C. Stedile, and J. R. Baumvol, J. Appl. Phys. **81**, 8109 (1997).

[90] Y. Inamura, M. Arai, N. Kitamura, S. M. Bennington, and A. C. Hannon, Physica B **241**, 903 (1998).

[91] R. M. C. de Almeida, S. Gonçalves, I. J. R. Baumvol, and F. C. Stedile, Phys. Rev. B **61**, 12 992 (2000).